Transformation of graphite into nanodiamond following extreme electronic excitations

A. Dunlop* and G. Jaskierowicz
Laboratoire des Solides Irradies, CEA-DRECAM/Ecole Polytechnique, 91128 Palaiseau, France

P. M. Ossi
Centre for NanoEngineered Materials and Surfaces—NEMAS, Politecnico di Milano, Milano, Italy

S. Della-Negra
Institut de Physique Nucléaire, CNRS-IN2P3, 91406 Orsay, France

(Received 30 January 2007; revised manuscript received 30 May 2007; published 2 October 2007)

Graphite targets have been irradiated at 90 K and 300 K with 850 MeV and 6 GeV lead ions and with 20–30 MeV fullerene cluster ions in a large range of fluences. Damage creation was studied both by transmission electron microscopy and Raman spectroscopy. The very strong energy density deposited in electronic processes generates a highly excited region around the projectile path. The relaxation of the deposited energy via hydrodynamic expansion and shock-wave propagation leads to the formation of small defective graphitic domains and of nanocrystalline diamond particles.

DOI: 10.1103/PhysRevB.76.155403 PACS number(s): 62.50.+p, 61.50.Ks

I. INTRODUCTION

This work is part of numerous studies concerning the structural modifications induced in various types of targets irradiated with energetic heavy projectiles. In this paper we will consider the case of a lamellar crystal, graphite, which has been extensively studied but in which damage creation and latent track formation are poorly understood. Atomic force microscopy (AFM) and scanning tunneling microscopy (STM) studies[1–4] performed on graphite irradiated with GeV heavy *monatomic* ions have shown that (i) tracks are formed much easier on the sample surface than in the bulk,[2] (ii) the damage along the ion path is discontinuous even for the highest stopping powers,[1,4] and (iii) the hillocks on the sample surface always have very small diameters in the range from 2 to 3 nm.[1,2] All these results point to the existence of a few discontinuous tracks of a very small diameter and could explain why they are so difficult to image using transmission electron microscopy (TEM).[5,6] Finally, a Raman spectroscopic study of irradiated graphite seems to indicate that after irradiation at a high fluence the damage leads to a decrease of the crystal domain size inside the track.[3]

We thus decided to study the damage induced in graphite by heavy energetic *cluster ions* in order to be in a regime of extremely high energy deposition which should lead to stronger structural modifications, possibly easier to characterize. As a matter of fact, at energies of a few MeV per nucleon, during their slowing down in the target, ions mainly deposit their energy via inelastic collisions with the target electrons leading to electronic excitations and ionizations. A lot of controversy exists in the literature concerning the detailed understanding of the mechanisms of conversion of the energy deposited in the electronic system into atomic displacements,[7–11] but it is clear that in close proximity to the projectile path a strongly excited cylindrical region is created. Dense excitations of the valence electrons around the ion path can cause an instability with respect to the high pressure phase of the target and to its atomic structure.[12] The relaxation of the excited matter induces permanent damage in the target and it has been shown that two parameters are decisive concerning the efficiency of damage production in such processes: (i) the linear rate of energy deposition in electronic processes $(dE/dx)_e$ and (ii) the projectile velocity v.[12–14] The stronger damage is observed for high $(dE/dx)_e$ and for slow projectiles, corresponding to the fact that the pertinent parameter describing these processes is the *density* of energy deposited in electronic processes.

Quite a few previous studies have clearly shown that the higher densities of electronic energy deposition are obtained using heavy clusters as projectiles.[15] In particular, the use of fullerene ions at energies of a few 10 MeV permitted to damage targets that were resistant to GeV monatomic ions and to create new damage structures: amorphous latent tracks in Si,[16,17] aligned dislocation loops in Fe,[18] phase change to the high pressure crystalline phase in Ti,[19] etc. We will thus first perform irradiations of graphite targets with energetic fullerene ions and study the damage using both TEM and Raman spectroscopy. In the last part of the paper new results concerning track creation by GeV monatomic heavy ions will shortly be described.

II. EXPERIMENT

Natural Sri Lankan and artificial graphite targets were prepared either by cleavage or by mechanical grinding in a mortar of massive material in order to get thin fragments (containing $\leqslant$100 nm thick regions) or very fine powder suitable for transmission electron microscopy observation. The fragments were deposited on 3 mm diameter copper grids which were either bare or covered with a very thin amorphous carbon layer. They were irradiated at normal incidence:

(i) At 300 K on the tandem accelerator in Orsay with 20 MeV and 30 MeV C_{60} cluster ions at fluences ranging from 3×10^9 to 3×10^{12} ions cm^{-2}. As no scanning of the beam is available on the irradiation line, the beam was slightly defocussed in order to irradiate rather homoge-

TABLE I. Irradiation parameters for TEM and Raman studies.

Projectile	Energy (MeV)	Irradiation temperature (K)	$(dE/dx)_e$ (keV/nm)	$(dE/dx)_n$ (eV/nm)	Fluence for TEM (ions cm^{-2})	Track diameter (nm)	Fluence for Raman studies (ions cm^{-2})
C_{60}	30	300	54.1	990	3×10^9 to 3×10^{12}	6.0	2.7×10^{11} (sample *C*)
C_{60}	20	300	44.6	1300	3×10^9 to 8×10^{11}	4.1	
Pb	850	90	26.2	48	1×10^{11} to 8×10^{11}	2 to 3	8×10^{11} (*A*) 8×10^{12} (*B*)
Pb	6000	90	16.9	9	3×10^{12} to 1×10^{13}	Not determined	

neously the central part ($\approx$4 mm^2) of the TEM grids. The ion flux was limited to 10^6 ions cm^{-2} s^{-1} in order to avoid any temperature increase and charging problem during the irradiations.

(ii) At 90 K on the GANIL facility in Caen with lead ions of 850 MeV and 6 GeV incident energies in the fluence range 1×10^{11} to 1×10^{13} ions cm^{-2}. The beam was scanned on a surface of a few cm^2 in order to ensure a homogeneous irradiation of the targets and the flux was again limited in order to control the target temperature during the irradiations.

When very energetic cluster ions hit a surface, they break up into single ions or smaller assemblies of ions. For C_{60} irradiations, the linear rates of energy deposition in electronic $(dE/dx)_e$ and nuclear $(dE/dx)_n$ processes were estimated as the sum of the energy loss of 60 individual carbon atoms of the same velocity.[20,21] The targets were examined at room temperature just after irradiation in a Philips CM 30 transmission electron microscope operating at 300 kV. The main experimental parameters are quoted in Table I.

To perform vibrational spectroscopy studies ($\approx$1 cm^2 in surface) massive samples and films of graphite were irradiated with 850 MeV Pb ions at 90 K (samples *A* and *B* in Table I) and with 30 MeV C_{60} at 300 K (sample *C* in Table I). Visible Raman spectra were taken under identical conditions, namely in backscattering geometry, using a triple-grating Jobin-Yvon T64000 spectrometer (1800 g/mm gratings). The excitation line with wavelength 532 nm from a frequency doubled ND-YAG Coherent DPSS 532 laser was used and the spectra were collected with a nitrogen-cooled CCD camera. The instrument spectral resolution was below 1 cm^{-1}. Unpolarized Raman spectra were recorded over the 400–1800 cm^{-1} wave-number range; the laser beam was filtered to avoid spurious peaks in the low wave-number region. As a rule, the spectra were taken from the center of the irradiated area of the sample surface, with the laser spot diameter on the sample fixed at 1 μm; in such a micro-Raman configuration the beam intensity is reduced by a factor of 2, the resulting laser energy at the sample surface being 50 mJ. The collection time for each spectrum was around 10 minutes. The deposited laser energy density does not induce surface modifications in graphite; this is confirmed by the absence of any change in the images of sample surface recorded by optical microscopy during laser irradiations, as well as by the reproducibility of different spectra subsequently recorded at the same position on the sample.

III. RESULTS FOR GRAPHITE IRRADIATED WITH 20 TO 30 MeV C_{60} CLUSTER IONS

A. Morphology of the tracks in conventional TEM conditions

After irradiation with energetic cluster ions, latent tracks are easily observed by transmission electron microscopy.

Figure 1, taken in focused conditions, shows a micrograph of a sample irradiated at 300 K by 30 MeV C_{60} ions up to a fluence of 2×10^{11} ions cm^{-2}. The density of dots corresponds to the ion fluence which indicates that each projectile generates a defective region around its path. The tracks have a *nonhomogeneous contrast*: some structures can be seen in the core of the tracks which are circled with a dark rim. The cross sections of the tracks have an average diameter of 6 nm. Figure 2 is relative to the same sample tilted by 20° in the microscope. The tracks have a constant diameter through the sample thickness and an *almost* uniform contrast.

Figure 3 presents a disalignment effect which is systematically observed in all the samples whatever the nature of

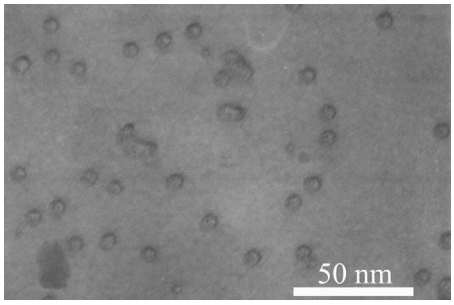

FIG. 1. Transmission electron micrograph of graphite irradiated at 300 K and at normal incidence with 30 MeV C_{60} ions up to a fluence of 2×10^{11} ions cm^{-2}.

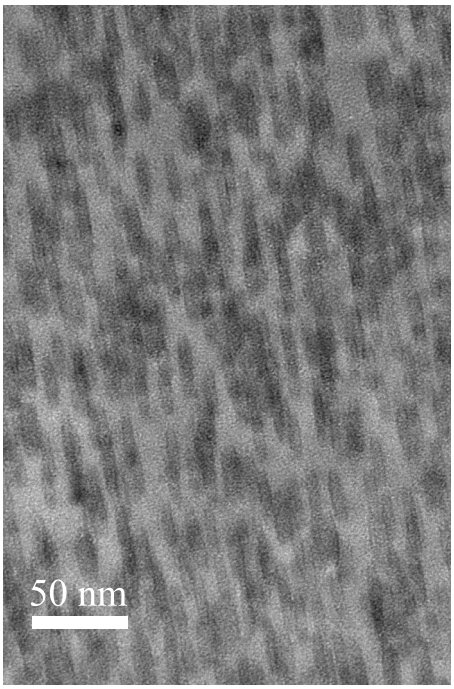

FIG. 2. Transmission electron micrograph of graphite irradiated at 300 K and at normal incidence with 30 MeV C_{60} ions up to a fluence of 2×10^{11} ions cm^{-2}. The sample is tilted by 20° in the electron microscope. No reflection excited.

the incident projectile. A significant disalignment of the axis of the tracks is observed (usually in the range from 6 to 9°) when the samples are tilted in the microscope. In the examples shown here the disorientation is 7° in Fig. 3(a) relative to 30 MeV C_{60} clusters and 6° in Fig. 3(b) relative to

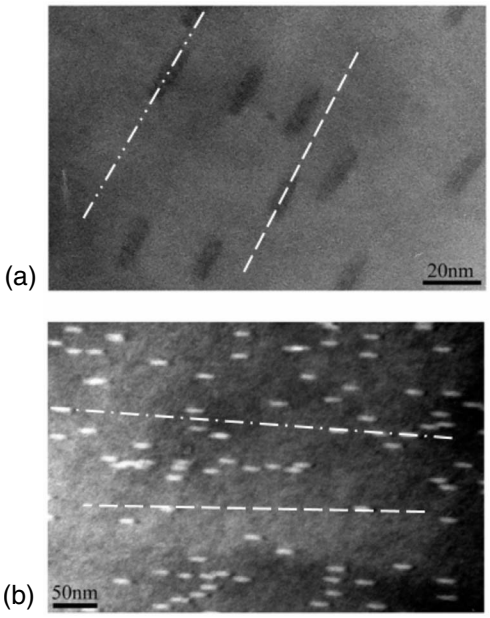

FIG. 3. Latent tracks induced at 300 K in graphite, respectively, by (a) 30 MeV and (b) 20 MeV C_{60} ions. The samples were tilted by 20° in the electron microscope. The discontinuous lines are drawn to help the visualization of the disalignment of the tracks.

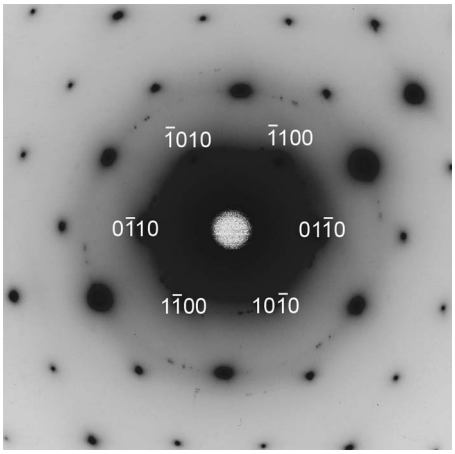

FIG. 4. Electron diffraction pattern recorded on a massive graphite sample irradiated at 300 K with 20 MeV C_{60} ions up to a fluence of 8×10^{11} ions cm^{-2}. Some of the main diffraction spots of graphite have been indexed.

20 MeV C_{60} clusters. This effect might be attributed to relaxation processes (occurring during or after irradiation) caused by the charging and/or the generation of internal stresses in the target during the irradiation.

Figure 4 is a typical electron diffraction pattern recorded after an irradiation of graphite at 300 K with 20 MeV C_{60} up to a high fluence (8×10^{11} clusters cm^{-2}). The characteristic spots of graphite are observed. Additional spots with low intensities characteristic of crystalline material can also be seen. *No diffuse ring that would be a signature of amorphous tracks is visible*. (This conclusion is deduced from previous observations of diffraction patterns obtained in similar conditions: for example, in $NiZr_2$ irradiated up to a fluence of 7×10^{11} ions cm^{-2} with Pb ions, amorphous tracks of 8 nm diameter are created and give rise to a diffuse ring with very high intensity in the diffraction pattern.[22]) This is confirmed by Fig. 5 showing the electron diffraction pattern of a sample of *powdered* graphite (fine powder deposited on a TEM copper grid covered with a very thin amorphous carbon film) irradiated at 300 K with 30 MeV C_{60} up to a fluence of 1×10^{11} clusters cm^{-2}. A large number of very fine new diffraction spots appear on the pattern [Fig. 5(a)]. They are located on rings corresponding to interplanar distances d_1 to d_4 [Fig. 5(b)].

B. Internal structure of the tracks

The morphology of the tracks induced in graphite is not as clear and simple as could be deduced from what is shown in Figs. 1 and 2. Depending on the diffraction conditions and on the sample region different features can be observed. For example, Fig. 6(c) is a micrograph taken in the same TEM grid as that from Fig. 1, but in another sample region. The tracks still have an average diameter of 6 nm but now have more irregular cross sections instead of the almost circular ones shown in Fig. 1. They still have a gray contrast in their center and a black rim. When tilted by 20° in the microscope [Fig. 7(a)], the contrast of the tracks is very inhomogeneous in the sample thickness and some structure is clearly seen

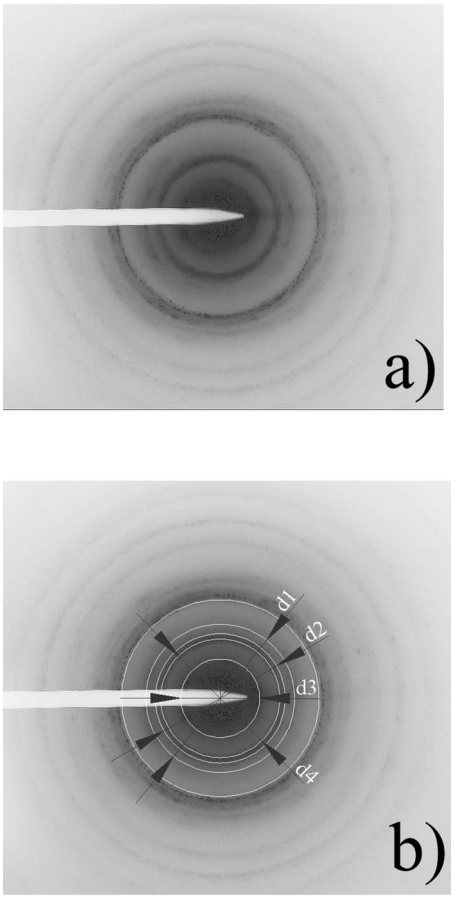

FIG. 5. Electron diffraction pattern recorded on a powdered graphite sample irradiated at 300 K with 30 MeV C_{60} ions up to a fluence of 10^{11} ions cm^{-2}. The original diffraction pattern shown in (a) is reproduced in (b) with circular lines lying on the new dotted diffraction spots induced by the irradiation. They correspond to interplanar distances: $0.085\ \text{nm} < d_1 < 0.086\ \text{nm}$, $0.097\ \text{nm} < d_2 < 0.099\ \text{nm}$, $0.161\ \text{nm} < d_3 < 0.162\ \text{nm}$, $0.106\ \text{nm} < d_4 < 0.108\ \text{nm}$.

along the track. This could be due to the presence of small disoriented crystallites in the track region. Very strong local variations of the diffraction conditions are frequently observed [Fig. 7(b)]. This could arise from (i) a different crystallographic structure inside the track and in the surrounding graphite and/or (ii) the existence of very important local stresses. *Just after irradiation*, nanocrystallites could thus exist in the track core.

The tracks created in graphite are extremely unstable under the electron beam and evolve very rapidly in the TEM. Figure 6 shows micrographs of tracks created in graphite by 20 MeV [Figs. 6(a) and 6(b)] and 30 MeV [Figs. 6(c) and 6(d)] C_{60} cluster ions as imaged when just introduced in the microscope [Figs. 6(a) and 6(c)] and after 2 minutes [Fig. 6(b)] or 5 minutes [Fig. 6(d)] in the TEM using a low electron current for observation. This change of contrast is systematically observed in all the samples which means that one must be very careful in order to know what was the internal structure of the tracks induced by the ion irradiation and study it before it has been modified by the electron beam. After observation in the TEM for a few minutes, the tracks

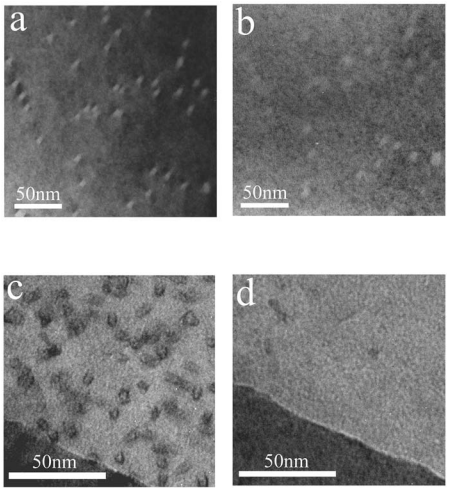

FIG. 6. Latent tracks induced at 300 K in graphite, respectively, by (a,b) 20 MeV and (c,d) 30 MeV C_{60} ions. Micrographs (a) and (c) were taken immediately after introducing the samples in the electron microscope, whereas micrographs (b) and (d) were registered after leaving a low current electron beam, respectively, during 2 or 5 minutes on the samples.

appear to have a very homogeneous contrast as is usually observed for amorphous tracks (Fig. 8).

Figure 9 presents a typical high resolution transmission electron micrograph of graphite irradiated by 30 MeV C_{60} ions at 300 K. When imaged in such conditions, the tracks always appear with a contrast that could be that of amorphous material. *Lattice fringes could never be imaged inside the tracks in such conditions*. It must be noted that the tracks undergo most probably a structural evolution under the electron beam. Amorphization of the *originally* crystalline tracks (as deduced from the electron diffraction pattern shown in Figs. 4 and 5) could well be induced by the focused electron

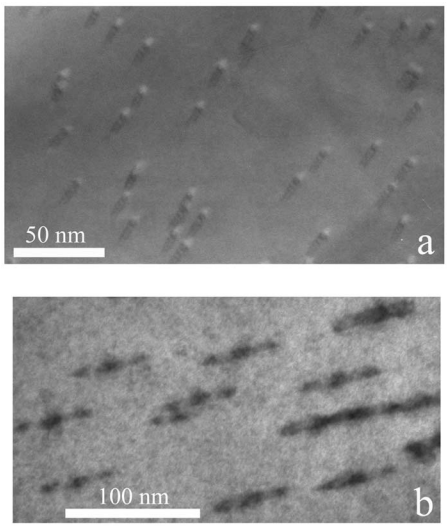

FIG. 7. Transmission electron micrographs of graphite irradiated at 300 K and at normal incidence with (a) 30 MeV C_{60} ions and (b) 20 MeV C_{60} ions. The samples were tilted by 20° in the electron microscope.

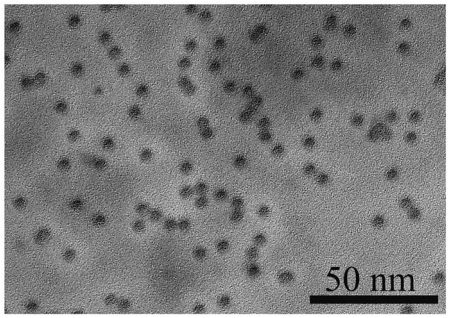

FIG. 8. Transmission electron micrographs of graphite irradiated at 300 K and at normal incidence with 30 MeV C_{60} ions. The micrograph is taken after a few minutes observation in the TEM.

beam used in the microscope for high resolution observations.

In all the samples that were deposited on a TEM grid covered with a very thin amorphous carbon film, numerous "objects" are in the vicinity of the graphite. These objects redeposited on the carbon foil are either sputtered from the entrance or exit surfaces of the tracks, or they are ejected as a whole from the track core. Two examples are shown in Fig. 10 after irradiation with 30 MeV C_{60}. Figure 10(a) shows an isolated "object" lying on the amorphous carbon film. In Fig. 10(b), the edge of the massive graphite sample is visible in the upper right-hand corner. Some impacts of cluster ions have damaged the amorphous carbon film (white contrasts) and a redeposited "object" is visible as a dark contrast. The diameters of these redeposited objects are in the range from 6 to 26 nm, which is on the average significantly larger than the track diameter (6 nm for 30 MeV C_{60} ions).

C. Structure of the redeposited material

First of all it must be noted that redeposited material lies also on the surface of the graphite samples. For the sake of simplicity, it is much easier to characterize the isolated objects lying on the carbon film than to study those redeposited on graphite. The redeposited material usually presents some

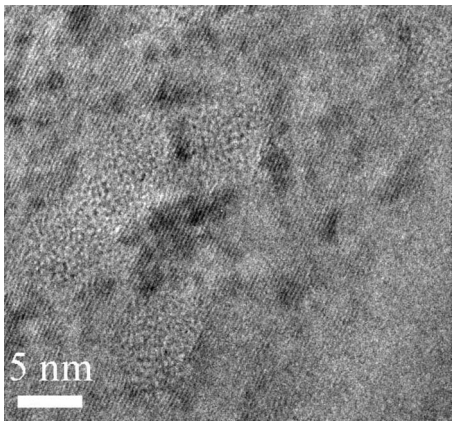

FIG. 9. High resolution transmission electron micrograph of graphite irradiated by 30 MeV C_{60} ions at 300 K.

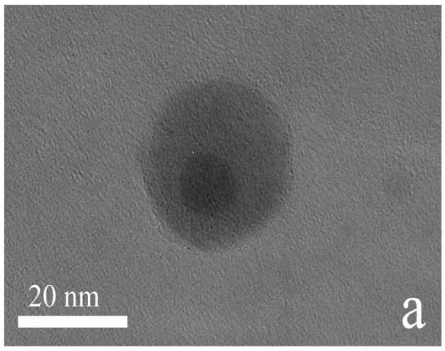

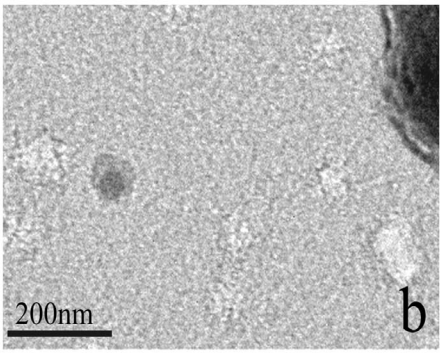

FIG. 10. Graphite sample deposited on a carbon covered TEM grid and irradiated at 300 K with 30 MeV C_{60} cluster ions up to a fluence of 5×10^{10} ions cm^{-2}.

darker contrast in the center (see Fig. 10). Contrarily to the tracks created in the bulk graphite, the ejected material is extremely stable under the electron beam. No evolution is seen during observation so that high resolution observations could be performed.

Figures 11–13 show typical high resolution micrographs of some nano-objects redeposited on the amorphous carbon

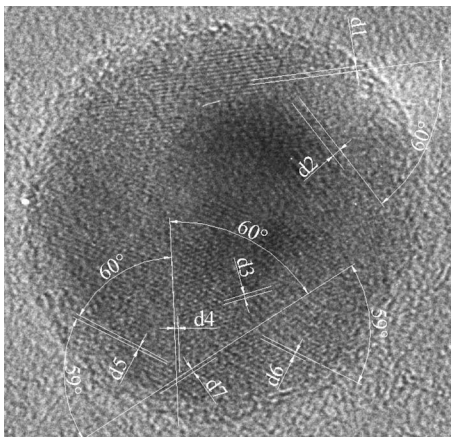

FIG. 11. High resolution transmission electron micrograph of graphite irradiated by 30 MeV C_{60} ions at 300 K up to a fluence of 5×10^{9} ions cm^2. The measured interplanar distances and angles are the following: $d_1=0.181$ nm, $d_2=0.334$ nm, $\theta(d_1,d_2)=60°$; $d_3=0.251$ nm, $d_4=0.247$ nm, $d_5=0.248$ nm, $d_6=0.250$ nm, $d_7=0.251$ nm, $\theta(d_4,d_5)=\theta(d_4,d_7)=60°$, $\theta(d_5,d_7)=\theta(d_6,d_7)=59°$.

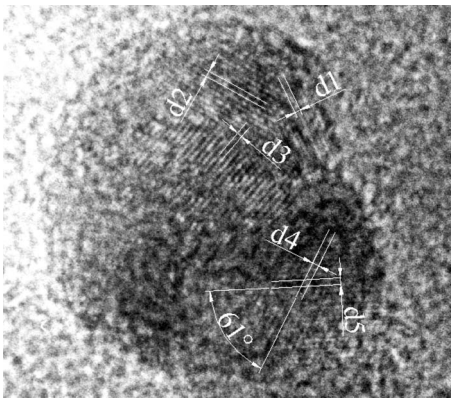

FIG. 12. High resolution transmission electron micrograph of graphite irradiated by 30 MeV C_{60} ions at 300 K up to a fluence of 5×10^9 ions cm^2. The measured interplanar distances and angle are the following: d_1=0.257 nm, d_2=0.250 nm, d_3=0.259 nm, d_4 =0.253 nm, d_5=0.255 nm, $\theta(d_4,d_5)$=61°.

FIG. 13. : High resolution transmission electron micrograph of graphite irradiated by 30 MeV C_{60} ions at 300 K up to a fluence of 10^{10} ions/cm^2. The measured interplanar distances and angle are the following: d_1=0.252 nm, d_2=0.261 nm, $\theta(d_1,d_2)$=59°, d_3 =0.250 nm.

film in the vicinity of graphite samples irradiated at 300 K with 30 MeV C_{60} ions. Measured interplanar distances and corresponding angles (see Table II) are quoted in the figure captions.

In Fig. 11, the upper right-hand part labelled with d_1 and d_2 corresponds to (012) and (002) planes of graphite, whereas the lower part labelled using d_3 to d_7 can be attributed to (110) planes of diamond. There is thus coexistence of the two crystalline phases in this particular object.

In Figs. 12 and 13, the measured interplanar distances and angles can only be attributed to diamond.

IV. RESULTS FOR GRAPHITE IRRADIATED WITH GeV LEAD IONS

In a previous preliminary work,[6] a detailed TEM study of graphite irradiated with GeV projectiles showed that a very strong ejection of matter and redeposition on the sample surfaces took place during irradiation with GeV Pb and U ions. No latent tracks could be imaged in this early work.

Following the results obtained with cluster projectiles, we decided to perform new irradiations with monatomic projectiles in order to search for latent track formation in the bulk and to analyze the redeposited material. Graphite was thus irradiated at 90 K with 850 MeV and 6 GeV Pb ions delivered by the GANIL accelerator in Caen (see Table I).

Figure 14 is a micrograph of graphite deposited on an amorphous carbon film and irradiated at 90 K with 6 GeV Pb ions up to a fluence of 3×10^{12} ions cm^{-2}. As previously observed there is a high number of redeposited nano-objects in the vicinity of the graphite target. Similarly to the study performed after irradiation with cluster ions, we recorded some high resolution images of nano-objects as shown in Figs. 15 and 16 and found very similar results. In Fig. 15, we could evidence the presence of diamond [(111) and (110) planes], whereas in Fig. 16, we find both diamond [d_1 and d_2=(110) planes of diamond] and graphite [d_3 and d_4 being attributed to (003) and (101) planes of graphite]. In a large number of the nano-objects we only found the graphite structure.

If we now observe samples irradiated at low fluences ($\cong10^{11}$ ions cm^{-2}) in order to image tracks in the bulk material, we find that the tracks are extremely difficult to observe as they give a very low contrast and are extremely unstable in the TEM. Moreover, the density of tracks that we observe is much smaller than the impinging ion fluence, which means that each ion does not generate a track which is visible in the TEM. Figure 17 shows tracks generated in graphite by 850 MeV Pb ions [$(dE/dx)_e$=26.2 keV/nm]. The tracks are seen from above in Fig. 17(a) and tilted in the TEM in Fig. 17(b). They give a very faint continuous contrast whereas surface studies[1,4] concluded to the probable existence of discontinuous tracks in this regime of $(dE/dx)_e$. Their average diameter was estimated to be of the order of 2 to 3 nm, which agrees well with the small hillock diameters measured by STM.[1,2] Finally, it must be noted that

TABLE II. Interplanar distances in graphite and diamond, and corresponding angles.

Graphite	d(002)	d(012)	d(003)	d(101)	θ(002), (012)	θ(003), (101)
	0.336 nm	0.180 nm	0.224 nm	0.204 nm	57°53	72°35
Diamond	d(100)	d(110)	d(111)	θ(111), (110)	θ(100), (110)	θ(110), (110)
	0.356 nm	0.252 nm	0.205 nm	90°	90° 45°	90° 60°

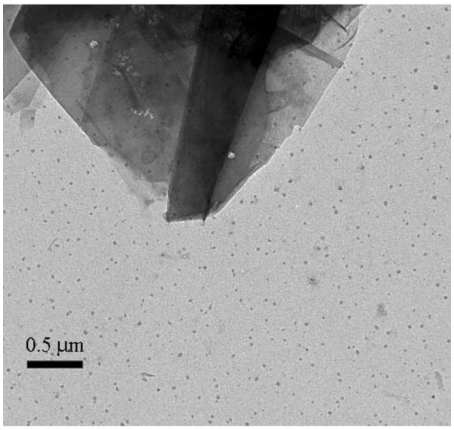

FIG. 14. Transmission electron micrograph of cleaved graphite deposited on an amorphous carbon film and irradiated at 90 K with 6 GeV Pb ions up to a fluence of 3×10^{12} ions cm^{-2}.

these results are in *complete disagreement* with a recent presentation[23] in which *very large* (20 nm diameter) *amorphous* tracks were imaged by TEM in graphite irradiated by 2.6 GeV U $[(dE/dx)_e=27$ keV/nm$]$. It is not clear at all what could be the origin of these contradictory results.

V. RAMAN SPECTROSCOPY

Raman spectroscopy is widely used to perform nondestructive structural analyses of materials and it was extensively adopted to study a large number of carbonaceous materials which were synthesized since the 1960s. Moving from the accumulated wealth of available Raman spectra of carbon-based materials a rather complicated picture of the correlation between the observed modifications of the features of Raman spectra and the material structure emerges. Thus, before discussing the spectral details of our samples it is useful to recall the main results in the field, in order of

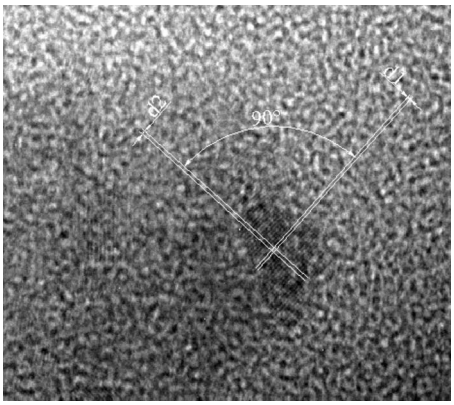

FIG. 15. High resolution transmission electron micrograph of cleaved graphite deposited on an amorphous carbon film and irradiated at 90 K with 6 GeV Pb ions up to a fluence of 3×10^{12} ions cm^{-2}. The interplanar distances measured in the redeposited material are $d_1=0.209$ nm, $d_2=0.259$ nm with $\theta(d_1,d_2)=90°$.

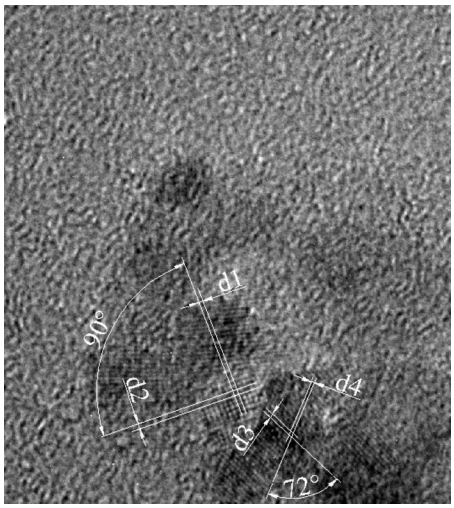

FIG. 16. High resolution transmission electron micrograph of cleaved graphite deposited on an amorphous carbon film and irradiated at 90 K with 6 GeV Pb ions up to a fluence of 3×10^{12} ions cm^{-2}. The interplanar distances measured in the redeposited material are $d_1=0.259$ nm, $d_2=0.253$ nm with $\theta(d_1,d_2)=90°$, $d_3=0.223$ nm, $d_4=0.201$ nm with $\theta(d_3,d_4)=72°$.

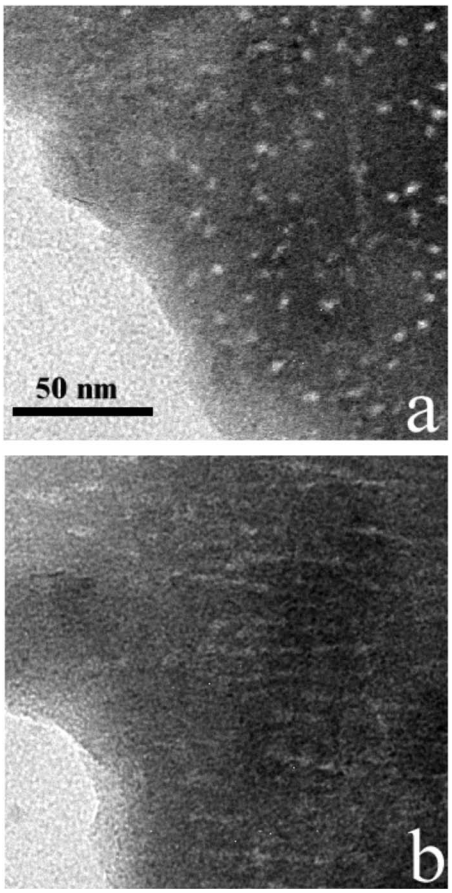

FIG. 17. Graphite irradiated at 90 K with 850 MeV Pb ions up to a fluence of 8×10^{11} ions cm^{-2}. Tracks seen from above (a), and after tilting by 20° in the microscope (b).

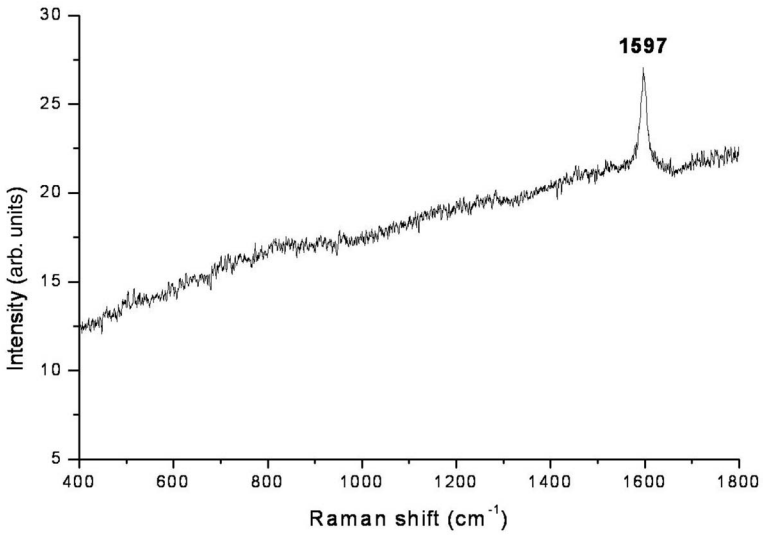

FIG. 18. Visible Raman spectrum of a graphite sample irradiated with 850 MeV Pb ions at a fluence of 8×10^{11} cm^{-2} (sample *A* in the text).

increasing complexity. The spectrum of sp^3 coordinated diamond consists of a single sharp peak at 1332 cm^{-1}, assigned to the zone center mode T_{2g}; in turn, sp^2 coordinated crystalline graphite displays a sharp peak (named *G* peak) at 1581 cm^{-1}, with E_{2g} symmetry. When graphite is increasingly disordered, the *G* peak broadens, as indicated by the FWHM value and a further feature (called *D* peak), which is attributed to *K*-point phonons with A_{1g} symmetry, is found at about 1350 cm^{-1} and becomes progressively better defined. *G* and *D* peaks, whose position and relative intensity change in different carbon-based materials, depending also on the preparation technique and post-preparation treatment, remain the leading features of all nanocrystalline and amorphous carbons, including those where an extended graphitic ordering is absent. Recently,[24] Raman spectroscopy data for a wide range of carbonaceous materials were systematically discussed and the trends of Raman parameters such as the position of the *G* peak and the intensity ratio between *D* and *G* peaks, $I_D I_G^{-1}$ were correlated to the structural evolution between the two extremes of graphite and tetrahedral amorphous carbon, where sp^3 coordination largely dominates. In so doing an indirect estimate of the fraction of sp^3-coordinated atoms in a disordered carbon network was provided. This is useful for practical purposes because visible Raman spectroscopy is by far [50 to about 200 times (Ref. 25)] more sensitive to sp^2 sites, whose π states are mostly excited by photons in the visible range than to sp^3 sites that can be directly probed only by ultraviolet (uv) photons with energy larger than 5.1 eV. Driven by the interest to artificially synthesize diamond, several routes have been explored producing nanocrystalline diamond particles and films with grain sizes mostly in the 5 to 100 nm range. The material forms only in the presence of energetic particles, e.g., from a plasma, impinging on the growing film with lower threshold energies around 100–200 eV. Particularly in the case of plasma enhanced CVD the carbonaceous material includes gaseous impurities such as hydrogen and nitrogen from the precursors used in the deposition process, even up to several tens atomic percent. Two companion peaks, around 1150 cm^{-1} and 1450 cm^{-1}, respectively, have been widely attributed to nanocrystalline diamond;[26] the origin of the two features however was recently questioned, being assigned to sum and difference combinations of C=C chain stretching and CH wagging modes in transpolyacetylene.[27] As to the diamond fingerprint at 1332 cm^{-1}, in low-quality, artificial nanodiamonds, it results in a very weak shoulder, if any, of the *D* peak, when a green light of 514 nm wavelength is used as the probe radiation.[27] When nanodiamond is observed as a result of a local transformation of shock-compressed graphite[28] the feature at 1332 cm^{-1}, if present, is embedded in the broad *D* peak of graphite.[29,30] Last, it is noteworthy that if graphite is shock compressed a transformation to diamond was locally observed;[28] the formation of tiny diamond particles is associated to the attainment of extreme temperature and pressure conditions, as discussed later. The Raman spectra of shock disordered graphite show, with increasing shock pressure in the range between 5 and 60 GPa, a redshift of both *D* and *G* peaks; the latter undergoes an intensity decrease and a broadening, while the intensity of the *D* peak increases. In the most heavily shocked graphite, experiencing local pressures above 45 GPa, an additional feature around 1400–1460 cm^{-1} is observed.[31]

We are now in a position to discuss the features observed in the visible Raman spectra of three representative graphite samples irradiated with 850 MeV Pb ions at 90 K up to fluences of 8×10^{11} ions cm^{-2} (sample *A*) and 8×10^{12} ions cm^{-2} (sample *B*) and with 30 MeV C_{60} at 300 K up to a fluence of 2.7×10^{11} cm^{-2} (sample *C*). The irradiation conditions for the three samples are reported in the last column of Table I.

Looking at the spectrum of sample *A*, as displayed in Fig. 18, the only well-defined feature is the narrow *G* band centered at 1597 cm^{-1} according to a Lorentzian fit to the Raman signal. The band full width at half-maximum (FWHM) is 17 cm^{-1}. From the literature we know that the *G* band lies between 1581 cm^{-1} in crystalline graphite and 1600 cm^{-1} in truly nanocrystalline graphite.[24] We conclude that the performed irradiation caused a transition from graphite to nanocrystalline graphite.

A higher fluence (sample *B*) significantly affects graphite structure; the effect is clearly recognizable in Fig. 19. The *G*

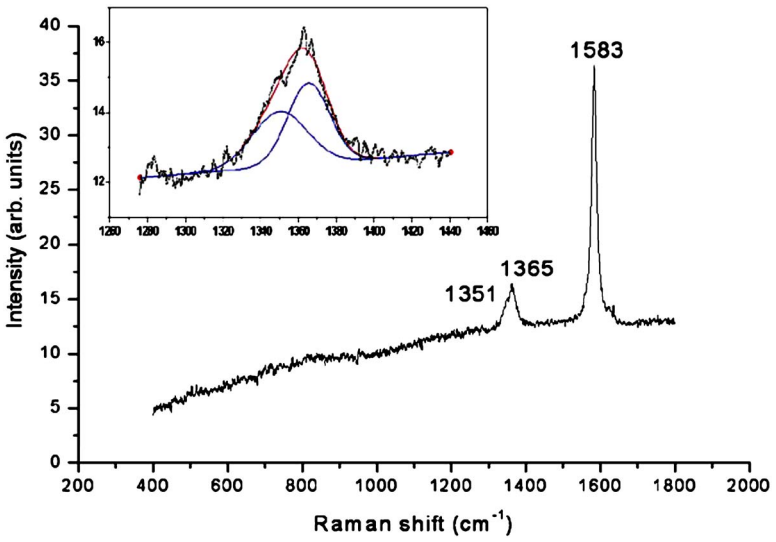

FIG. 19. (Color online) Visible Raman spectrum of a graphite sample irradiated with 850 MeV Pb ions at a fluence of 8×10^{12} cm^{-2} (sample *B* in the text).

peak undergoes a redshift with the maximum at 1583 cm^{-1} (FWHM=15.8 cm^{-1}); correspondingly a broad, asymmetric *D* peak is found, with an evident shoulder on the low wavenumber side. From a Gaussian fit to the *D* peak, as shown in the inset of Fig. 19, the low frequency component is centered at 1351 cm^{-1}, while the peak maximum is at 1365 cm^{-1}. A considerable degree of structural disorder was induced in graphite by irradiation; this is responsible for the presence, position, and intensity of the *D* peak. From the ratio of peak intensities $I_D I_G^{-1}=0.22$ the coherence length L_a of cooperatively scattering graphitic domains[32] is 20 nm. Besides this, the shoulder at 1351 cm^{-1}, as already observed,[30,33] indicates the presence of nanocrystalline diamond particles that were most likely formed upon ion bombardment.

Four Raman spectra were taken on sample *C* at different positions, according to optical microscopy observations of sample surface, that appears not uniformly damaged. From a position out of the C_{60} line of sight, near the sample lateral side, the spectrum (not reported) consists of the *G* peak alone, centered at 1589 cm^{-1}, with FWHM=14 cm^{-1}; this is essentially identical to the spectrum in Fig. 18 and can be assigned to a crystalline-nanocrystalline transition of graphite; the narrower *G* peak indicates that the extent of such a transition is less than in sample *A*.

Moving towards the center of the sample, from a zone that appears not evidently defected we collected the spectrum displayed in Fig. 20. Its main features are the *G* peak at 1584 cm^{-1} (FWHM=15 cm^{-1}) and the very broad, low intensity *D* peak, with a maximum at 1365 cm^{-1} and a shoulder at 1349 cm^{-1}. Besides this there is a small feature at 1641 cm^{-1}; the latter is the so-called *D′* peak that is a further signature of structural disordering of graphitic domains. From $I_D I_G^{-1}=0.05$, the coherence length is $L_a=88$ nm. The position of the shoulder at 1349 cm^{-1} is again within the range reported for the feature associated to the presence of nanocrystalline diamond (see the discussion of sample *B*). The weak band at about 482 cm^{-1} that was observed only in this spectrum is presently unexplained. Indeed, from its position it could be attributed to C_{60}, or to sizeable C_{60} fragments. However, clusters impacting onto a solid surface at the high energy adopted here are completely destroyed;[34] even if a considerable number of C_{60} fragments with appre-

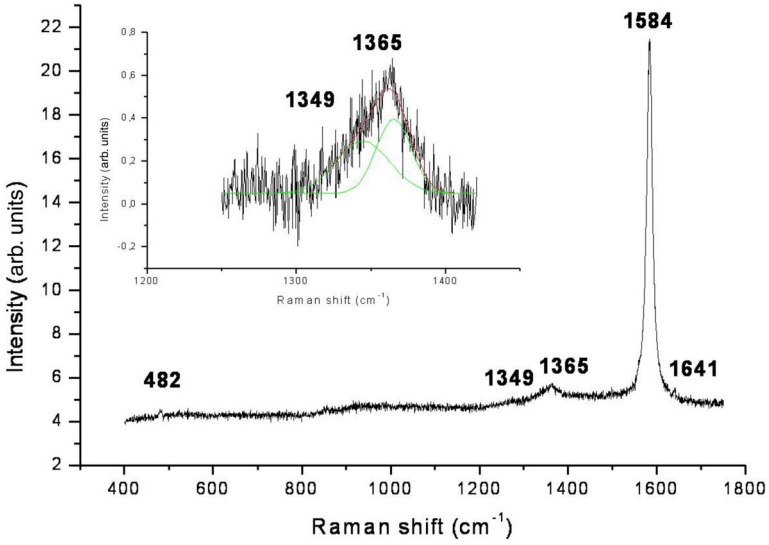

FIG. 20. (Color online) Visible Raman spectrum of a not evidently damaged area of a graphite sample irradiated with 30 MeV C_{60} at a fluence of 2.7×10^{11} cm^{-2} (sample *C* in the text). The inset shows the fit to the *D* peak. Notice the small feature at 482 cm^{-1}.

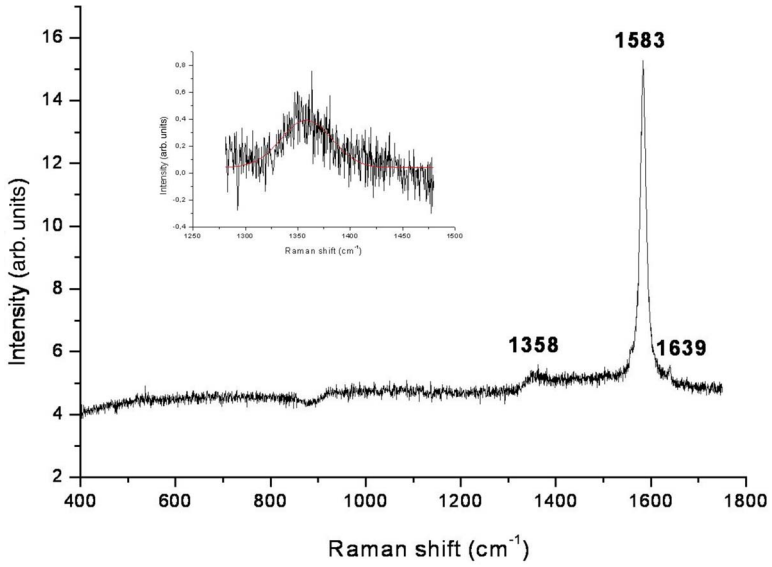

FIG. 21. (Color online) Visible Raman spectrum from a near-center zone of a graphite sample irradiated with 30 MeV C_{60} at a fluence of 2.7×10^{11} cm^{-2} (sample *C* in the text). The inset shows the fit to the *D* peak.

ciable size survived the impact, they should give at least another feature at about 1470 cm^{-1},[35] which however is not observed at all in the spectrum. Finally, the probability that after the impact C_{60} units reform in the irradiated region of the target is vanishingly small, besides being kinetically unfavored, given the too brief relaxation time with respect to C_{60} nucleation time.

The Raman spectrum shown in Fig. 21 was taken at a position of the sample surface slightly more displaced towards the center. The spectrum is in substantial agreement with that in Fig. 20 and consists of the *G* (FWHM $=14.9$cm^{-1}), the *D′* and the *D* peaks, at the positions marked in the figure. The oscillation of the background signal around 850–950 cm^{-1} is an artifact. The inset shows the fitting to the *D* peak, from which a single broad maximum is identified at 1358 cm^{-1}. From the intensity ratio $I_D I_G^{-1}=0.09$ the deduced L_a value is 49 nm. The overall indication is that upon C_{60} irradiation increasingly more severe disorder is found in sample zones progressively nearer to its center.

Optical microscopy observation of the center of sample *C* shows a dark, heavily defected surface. The corresponding Raman spectrum is reported in Fig. 22. From a luminescence background four main features grow up, at 1100, 1363, 1443, and 1582 cm^{-1}. Two of them, as already discussed, are the *G* (1582 cm^{-1}, FWHM$=$21.8 cm^{-1}) and *D* (1363 cm^{-1}) peaks of disordered, nanocrystalline graphite; from the ratio $I_D I_G^{-1}=0.34$, the coherence length is $L_a=12.9$ nm. The shoulder of the *D* peak at 1348 cm^{-1} is again attributable to nanocrystalline diamond. In this spectrum such a signature is accompanied by the broad, but evident band centered around 1100 cm^{-1}, corresponding to the peak often observed around 1150 cm^{-1}, in turn attributed to nanocrystalline diamond,[26] redshifted by the shock pressure induced by impacting clusters. Coming back to our introductory discussion, this feature was attributed to transpolyacetylene, together with its companion band around 1450 cm^{-1};[28] however, in our samples, that were irradiated under careful ambient control, there is no hydrogen, so transpolyacetylene is simply absent. Thus the

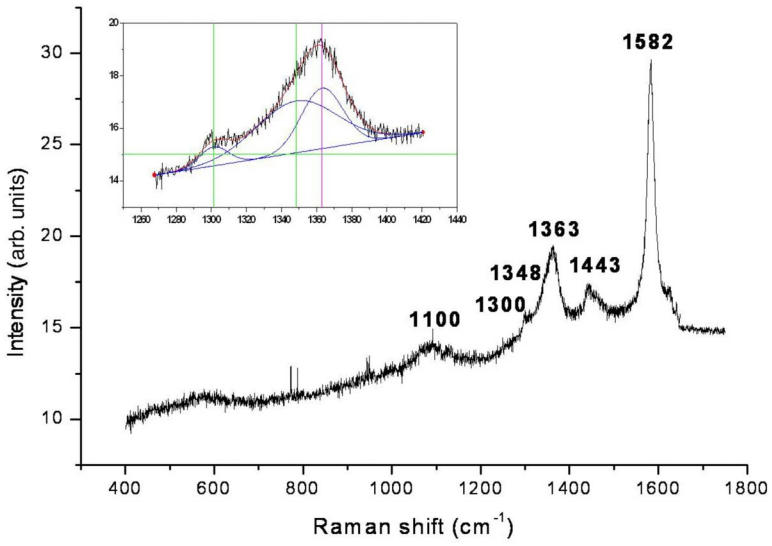

FIG. 22. (Color online) Visible Raman spectrum from the center of a graphite sample irradiated with 30 MeV C_{60} at a fluence of 2.7×10^{11} cm^{-2} (sample *C* in the text). The inset shows the fit to the *D* peak. Notice the features at 1100 and 1443 cm^{-1}, indicating that graphite was heavily shocked.

TABLE III. Interplanar distances in graphite and diamond (nm).

Interplanar distances deduced from additional spots in Fig. 5	Graphite	Diamond
$0.085\ \text{nm} < d_1 < 0.086\ \text{nm}$		$d(411)=d(330)=0.084$ $d(322)=d(410)=0.086$
$0.097\ \text{nm} < d_2 < 0.099\ \text{nm}$	$d(023)=0.097$ $d(114)=0.099$	$d(320)=0.099$
$0.161\ \text{nm} < d_3 < 0.162\ \text{nm}$		$d(210)=0.160$
$0.106\ \text{nm} < d_4 < 0.108\ \text{nm}$	$d(200)=0.107$ $d(113)=0.108$	$d(311)=0.107$

argument against the attribution of the features in question to nanocrystalline diamond, although plausible in the framework of CVD deposited films, seems to have nongeneral validity. Instead, in agreement with previous Raman spectroscopy of heavily shocked graphite, the feature we observe at 1443 cm^{-1} is possibly caused by the metastable carbon phase consisting of a chain of alternate single-triple C-C bonds known as carbyne, or equivalently, as chaoite.[31] Finally, the small feature at 1300 cm^{-1} could arise from the redshifted diamond feature at 1332 cm^{-1}.

Thus, according to the Raman spectrum just discussed, at least some zones of sample *C* experienced severe repeated shock impacts that brought crystalline graphite to local pressure-temperature conditions favorable to the synthesis both of nanocrystalline diamond and presumably of carbyne.

Summarizing, the coherent picture that emerges from the bulk of Raman observations is that the structural evolution of samples that suffered progressively increasing irradiation induced disorder can be discussed starting from graphite as the reference to explain the changes of Raman features; the *D* peak is due to aromatic rings and $I_D I_G^{-1}$ value increases with increasing disorder. The shoulder of the *D* on the low wavenumber side is a signature of nanocrystalline diamond formation and it is observed together with the features at 1100 and 1443 cm^{-1} only in the most heavily disordered material where the energy density released during subsequent impacts is the highest.

VI. DISCUSSION AND CONCLUSIONS

Let us first of all summarize the experimental findings: (i) latent tracks are created in graphite after irradiation with GeV Pb ions and with 20 to 30 MeV C_{60} ions and were observed using TEM, (ii) in both types of irradiations a large number of nanoclusters are ejected and are found lying on the sample surface or on the amorphous carbon foil supporting the graphite material, (iii) the tracks created in the bulk graphite are very unstable under the electron beam whereas the nanoclusters do not evolve in the TEM. It is thus very difficult to determine the nature of the modified matter along the projectile path.

Nevertheless we can conclude that, just after irradiation, being careful to avoid any evolution in the TEM (e.g., the observation conditions of Fig. 8 *certainly resulted in such an evolution*), tracks are crystalline in nature as deduced from TEM micrographs (Figs. 1 and 7) and diffraction patterns (Figs. 4 and 5). Table III shows the interplanar distances corresponding to additional spots observed after irradiation on the diffraction pattern shown in Fig. 5 together with interplanar distances in both graphite and diamond structures. It is clear from the table that lines d_1 and d_3 *can only be attributed to diamond*, whereas an ambiguity subsists for lines d_2 and d_4 which can correspond either to diamond or graphite. In turn, Raman spectroscopy shows a definite structural evolution towards nanodiamond and disordered graphite with increasing deposited energy density.

Finally, let us recall that in the isolated nanoparticles found in the vicinity of the graphite target, a similar result is found: the high resolution micrographs show the coexistence of both diamond and graphite in some of them and the presence of diamond only in others. This result is not surprising as in all the previous studies[23,36] in which one could clearly identify both the structure of the damaged track regions included in the target matrix and that of the redeposited material in the vicinity of the target, they were found to be the same. This was, for example, the case for amorphization of $Y_3Fe_5O_{12}$ (Ref. 37) or for the formation of concentric onions in MoS_2.[36] The tracks created in the bulk of graphite could thus consist of a *mixture of graphite and diamond of nanometer sizes*.

These tracks including small diamond crystallites are quite unstable when they are surrounded by the graphite matrix, so that even the small amount of energy used for TEM observation is sufficient to induce some structural modification. At the opposite, when the nano-objects lie in an isolated state on the amorphous carbon film, they do not show any visible structural modification under the electron beam. This behavior must be considered in the scope of the results of Badziag[38] who showed that surface energies play a very important role to the stabilization of microcrystalline diamonds. It was also pointed out by Daulton[39] that taking into account these surface energy considerations and the fact that there is a very small difference between graphite and diamond free energies, *diamond might be the stable phase at very small particle sizes*.

If we consider the carbon phase diagram in Fig. 23, it is clear that the transformation of graphite *G* into diamond *D* needs both high temperatures and pressures. As a matter of fact, numerous presentations show that the $G \rightarrow D$ transfor-

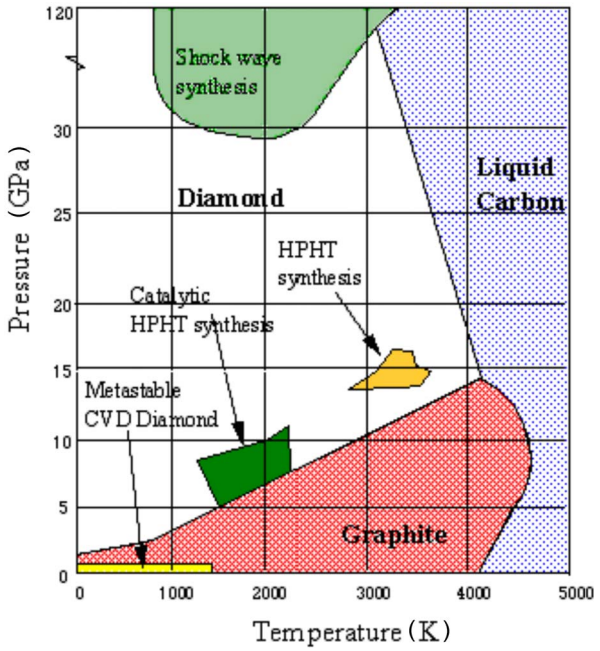

FIG. 23. (Color online) Pressure-temperature phase diagram of carbon (from Ref. 40).

mation in shock experiments needs pressures of the order of 30 to 40 GPa in agreement with the line drawn in the upper part of Fig. 23. Moreover, intense shock loading is inevitably accompanied by high temperatures.[41] Notice that even when bombarding particles are absent, such as when irradiating with intense uv laser pulses highly oriented pyrolytic graphite, a TEM analysis of the irradiated target showed the presence of sherelike nanocrystalline diamond particles formed when a shock wave was generated towards the bulk of the target upon violent evaporation of a cloud of particles (atoms and small clusters) from the molten surface layer.[42] As reported in Ref. 43, during shock-compression experiments, "only small particles of diamond can be produced because of the very short time at high temperature and pressure and the necessity for the individual particles to be small in order to satisfy the fast thermal quench requirement." The formation of diamond from graphite in meteorite impact craters was also estimated to have occurred at peak shock pressures between 30 and 40 GPa.[44] The shock-wave electrodynamic compression of graphite in the laboratory up to similar pressures leads to the formation of polycrystalline diamond grains up to 1 μm in size.[45]

Can such pressure waves be generated during irradiation experiments? As quoted in Ref. 46 the high temperature and pressure gradients obtained under cluster impacts are comparable to those obtained for meteorite-planet impacts.[47] Information can be found in the literature concerning the generation of pressure waves when high rates of electronic excitation are created in the irradiated targets. Computer simulation studies[48–50] show that following electronic excitations, a radial pressure wave moves outwards from the track core and that this pressure pulse carries away an important fraction of the deposited energy. Structural modifications and phase changes can occur during this expansion process.[48] More precisely, during irradiation of pure titanium with pulsed power beams (400 keV H and C) the stress generated by the pulse was estimated to reach 14 GPa.[51] Recently, the impact of neutral carbon clusters accelerated only at hyperthermal energies resulted in the development of metastable carbyne chains embedded in a growing graphitic film, with enough abundance to allow for reliable Raman measurements.[52] A subsequent calculation showed that the *same* narrow window of average energy per particle gives rise to carbyne chain formation during thin film deposition and in ancient meteorite impacts on the Earth, such as the one that resulted in Ries crater.[53] *The irradiation with MeV fullerene ions (and to a smaller extent with GeV monatomic heavy ions) certainly generates very intense outgoing recoil pressure pulses that induce the graphite→diamond phase change*.

In the literature, one can find a small number of irradiation experiments leading to generation of diamond from graphite:

(i) The first kind of experiment concerns irradiations *at high temperatures* of carbon graphitic material. When carbon onions are heated at 700 °C and irradiated in a TEM with an intense focused electron beam, the outer graphitic shells act as nanoscopic pressure cells.[54,55] The pressure in the onion core can reach up to 100 GPa which allows the nucleation of a diamond in the core. It must be noticed that the transformation is induced by the high number of *individual atomic displacements* produced by the electron irradiation.

The other case concerns the transformation of carbon onions into diamond following irradiation at 700 °C–1000 °C with 3 MeV Ne ions using a very high current density.[56] The accumulation of damage generated *in collision cascades* leads again to the generation of a diamond core.

For both these studies, *very high irradiation fluences*, corresponding to some 600 displacements per carbon atom are necessary.

(ii) The second[39] is an irradiation at room temperature of graphite sheets with 350 MeV Kr $[(dE/dx)_e=9$ keV/nm] ions to high fluences of 6×10^{12} ions cm^{-2}. Damage is now produced in "tracks" surrounding the ion trajectories. The irradiated samples were subjected to acid dissolution and the residues were characterized by TEM. Nanodiamonds of an average diameter of 7.5 nm were found, but it must be emphasized that in these conditions they were produced with a *very low efficiency* as the measured yield is of 0.01 diamond/ion. The conclusion of the authors is that nanodiamonds must develop instantaneously in single ion tracks and that their formation is a rare event. The experimental technique does not allow to know whether these diamond crystals come from the track cores or from ejected or sputtered material.

Considering now our own results, we were able to show the presence of nanodiamonds after irradiation of graphite at 90 K with GeV lead ions and at *room temperature* with energetic fullerene ions. The nanodiamonds were found by TEM already after irradiation at *low fluences* (a few 10^9 ions cm^2 as shown in Figs. 11–13) in material ejected from the track core or sputtered from the sample surface, which shows that the phase change occurs in the vicinity of each projectile path. The latent tracks have a diameter of

6 nm after irradiation with 30 MeV fullerene. They are crystalline and consist most probably of a mixture of small crystals of both defective graphite and diamonds. The coexistence of crystalline disordered graphitic nanodomains and of nanocrystalline diamond particles is confirmed by Raman spectroscopy. Such an evolution of the sample structure is a consequence of the *rapid* deposition of *extremely high energy densities* during the irradiations. In such conditions, energy transport from the excited region can occur by shock propagation and by a hydrodynamic expansion that causes the ejection of material from the solid.[57] The generation and propagation of an intense shock-wave accompanied by strong temperature increases leads to the fragmentation of the target in small domains[3] and to a phase transition to diamond[41] which is favored by the fact that diamond seems to be the more stable phase at very small particle sizes.[39]

*Corresponding author; annie.dunlop@polytechnique.fr

[1] S. Bouffard, J. Cousty, Y. Pennec, and F. Thibaudau, Radiat. Eff. Defects Solids **126**, 225 (1993).
[2] J. Liu, R. Neumann, C. Trautmann, and C. Müller, Phys. Rev. B **64**, 184115 (2001).
[3] J. Liu, M. D. Hou, C. Trautmann, R. Neumann, C. Müller, Z. G. Wang, Q. X. Zhang, Y. M. Sun, Y. F. Yin, H. W. Liu, and H. J. Gao, Nucl. Instrum. Methods Phys. Res. B **212**, 303 (2003).
[4] J. Liu, C. Trautmann, C. Müller, and R. Neumann, Nucl. Instrum. Methods Phys. Res. B **193**, 259 (2002).
[5] L. T. Chadderton, D. Fink, E. G. Gamaly, H. Moeckel, L. Wang, H. Omichi, and F. Hosoi, Nucl. Instrum. Methods Phys. Res. B **91**, 7 (1994).
[6] A. Dunlop, G. Jaskierowicz, and L. T. Chadderton, Nucl. Instrum. Methods Phys. Res. B **145**, 532 (1998).
[7] R. L. Fleischer, P. B. Price, and R. M. Walker, J. Appl. Phys. **36**, 3645 (1965).
[8] D. Lesueur and A. Dunlop, Radiat. Eff. Defects Solids **126**, 163 (1993).
[9] M. Toulemonde, C. Dufour, and E. Paumier, Phys. Rev. B **46**, 14362 (1992).
[10] A. E. Volkov and V. A. Borodin, Nucl. Instrum. Methods Phys. Res. B **193**, 381 (2002).
[11] E. M. Bringa and R. E. Johnson, Phys. Rev. Lett. **88**, 165501 (2002).
[12] P. Stampfli, Nucl. Instrum. Methods Phys. Res. B **107**, 138 (1996).
[13] A. Meftah, F. Brisard, J. M. Costantini, M. Hage-Ali, J. P. Stoquert, F. Studer, and M. Toulemonde, Phys. Rev. B **48**, 920 (1993).
[14] J. Jensen, A. Dunlop, S. Della Negra, and M. Toulemonde, Nucl. Instrum. Methods Phys. Res. B **146**, 412 (1998).
[15] H. Dammak, A. Dunlop, D. Lesueur, A. Brunelle, S. Della-Negra, and Y. Le Beyec, Phys. Rev. Lett. **74**, 1135 (1995).
[16] B. Canut, N. Bonardi, S. M. M. Ramos, and S. Della Negra, Nucl. Instrum. Methods Phys. Res. B **146**, 296 (1998).
[17] A. Dunlop, G. Jaskierowicz, and S. Della Negra, Nucl. Instrum. Methods Phys. Res. B **146**, 302 (1998).
[18] H. Dammak and A. Dunlop, Nucl. Instrum. Methods Phys. Res. B **146**, 285 (1998).
[19] M. Angiolini, H. Dammak, and A. Dunlop, Philos. Mag. Lett. **82**, 81 (2002).
[20] K. Baudin, A. Brunelle, M. Chabot, S. Della-Negra, J. Depauw, D. Gardès, P. Hakansson, Y. Le Beyec, A. Billebaud, M. Fallavier, J. Remillieux, J. C. Poizat, and J. P. Thomas, Nucl. Instrum. Methods Phys. Res. B **94**, 341 (1994).
[21] Ch. Tomaschko, D. Brandl, R. Kügler, M. Schurr, and H. Voit, Nucl. Instrum. Methods Phys. Res. B **103**, 407 (1995).
[22] A. Barbu, A. Dunlop, D. Lesueur, and R. S. Averback, Europhys. Lett. **15**, 37 (1991).
[23] U. A. Glasmacher, M. Lang, H. Keppler, F. Langenhorst, R. Neumann, D. Schardt, C. Trautmann, and G. A. Wagner, Phys. Rev. Lett. **96**, 195701 (2006).
[24] A. C. Ferrari and J. Robertson, Phys. Rev. B **61**, 14095 (2000).
[25] S. R. Salis, D. J. Gardiner, M. Bowden, J. Savage, and D. Rodway, Diamond Relat. Mater. **5**, 589 (1996).
[26] R. J. Nemanich, J. T. Glass, G. Lucovsky, and R. E. Schroder, J. Vac. Sci. Technol. A **6**, 1783 (1988).
[27] A. C. Ferrari and J. Robertson, Phys. Rev. B **63**, 121405(R) (2001).
[28] R. M. Hough, I. Gilmour, C. T. Pillinger, J. W. Arden, K. W. R. Gilkess, J. Yuan, and H. J. Milledge, Nature (London) **378**, 41 (1995).
[29] C. Lapke, R. T. Schmitt, T. Kenkmann, and D. Stöffler, Meteorit. Planet. Sci. **35**, 95 (2000).
[30] J. B. Wang, C. Y. Zhang, X. L. Zhong, and G. W. Yang, Chem. Phys. Lett. **361**, 86 (2002).
[31] A. El Goresy and G. Donnay, Science **161**, 363 (1968).
[32] F. Tuinstra and J. L. Koening, J. Chem. Phys. **53**, 1126 (1970).
[33] Z. Qiao, J. Li, N. Zhao, C. Shi, and P. Nash, Chem. Phys. Lett. **429**, 479 (2006).
[34] G. Betz and W. Husinsky, Nucl. Instrum. Methods Phys. Res. B **122**, 311 (1997).
[35] D. S. Bethune, G. Meijer, W. C. Tang, H. J. Rosen, W. G. Golden, H. Seki, C. A. Brown, and M. S. de Vries, Chem. Phys. Lett. **179**, 181 (1991).
[36] J. Henry, A. Dunlop, and S. Della Negra, Nucl. Instrum. Methods Phys. Res. B **146**, 405 (1998).
[37] A. Dunlop, G. Jaskierowicz, J. Jensen, and S. Della Negra, Nucl. Instrum. Methods Phys. Res. B **132**, 93 (1997).
[38] P. Badziag, W. S. Verwoerd, W. P. Ellis, and N. R. Greiner, Nature (London) **343**, 244 (1990).
[39] T. L. Daulton, M. A. Kirk, R. S. Lewis, and L. E. Rehn, Nucl. Instrum. Methods Phys. Res. B **175**, 12 (2001).
[40] F. P. Bundy, J. Geophys. Res. B **85**, 6930 (1980).
[41] S. S. Batsanov, High Pressure Crystallography, Erice summer school, 2003 pp. 307–318.
[42] M. Bonelli, A. Miotello, P. M. Ossi, A. Pessi, and S. Gialanella, Phys. Rev. B **59**, 13513(R) (1999).
[43] F. P. Bundy, W. A. Bassett, M. S. Weathers, R. J. Hemley, H. K. Maoand, and A. F. Goncharov, Carbon **34**, 141 (1996).
[44] A. El Goresy, P. Gillet, M. Chen, F. Künstler, G. Graup, and V. Stähle, Am. Mineral. **86**, 611 (2001).
[45] I. P. Makarevich, A. D. Rakhel, B. V. Rumyantsev, and B. E.

Fridman, Phys. Solid State **46**, 675 (2004).
[46] V. N. Popok and E. E. B. Campbell, Rev. Adv. Mater. Sci. **11**, 19 (2006).
[47] H. J. Melosh, *Impact Cratering: A Geologic Process* (Oxford University Press, New-York, 1989).
[48] E. M. Bringa and R. E. Johnson, Nucl. Instrum. Methods Phys. Res. B **146**, 513 (1998).
[49] E. M. Bringa, M. Jakas, and R. E. Johnson, Nucl. Instrum. Methods Phys. Res. B **164-165**, 762 (2000).
[50] M. M. Jakas and E. M. Bringa, Phys. Rev. B **62**, 824 (2000).
[51] V. Laurentiev, C. Hammerl, B. Rauschenbach, A. Pisanenko, and O. Kukharenko, Philos. Mag. A **81**, 511 (2001).
[52] L. Ravagnan, F. Siviero, C. Lenardi, P. Piseri, E. Barborini, P. Milani, C. S. Casari, A. Li Bassi, and C. E. Bottani, Phys. Rev. Lett. **89**, 285506 (2002).
[53] A. Lamperti and P. M. Ossi, Chem. Phys. Lett. **376**, 662 (2003).
[54] F. Banhart and P. M. Ajayan, Nature (London) **382**, 433 (1996).
[55] F. Banhart, J. Appl. Phys. **81**, 3440 (1997).
[56] P. Wesolowski, Y. Lyutovich, F. Banhart, H. D. Carstanjen, and H. Kronmüller, Appl. Phys. Lett. **71**, 1948 (1997).
[57] D. Fenyö and R. E. Johnson, Phys. Rev. B **46**, 5090 (1992).